

High-temperature flow behavior modeling of 2099 alloy considering strain effects

Fei ZHANG^{1,2}, Jian SHEN¹, Xiao-dong YAN¹, Jian-lin SUN², Xiao-long SUN¹, Yin YANG¹, Yong LIU³

1. General Research Institute of Nonferrous Metals, Beijing 100088, China;

2. School of Materials Science and Engineering, University of Science and Technology Beijing, Beijing 100083, China;

3. Southern Air Power Machinery Group Co., Ltd., Zhuzhou 412000, China

Received 6 March 2013; accepted 30 May 2013

Abstract: Isothermal compression tests in a wide range of temperatures (300–500 °C) and strain rates (0.001–10 s⁻¹), were performed on 2099 alloy to reveal the hot deformation characteristics. In order to give a precise prediction of flow behavior, the obtained experimental data were modified by friction and temperature correction and then employed to derive the constitutive modeling. The effects of the temperature and strain rate on hot deformation behavior can be expressed by Zener–Hollomon parameter including Arrhenius term. Furthermore, the influence of strain was incorporated in the constitutive analysis by considering the effect of strain on material constants (i.e. α , n , Q and A). Consequently, the flow stress curves predicted by the developed modeling show a good agreement with the corrected ones, which indicates that the developed constitutive modeling could give an accurate and precise prediction for the flow stress of 2099 alloy.

Key words: 2099 alloy; constitutive modeling; compensation of strain; flow stress

1 Introduction

Aluminum–lithium (Al–Li) alloys are used commercially in military aircraft and space vehicles in several critical applications. There is still, however, an interest in developing the next generation of Al–Li alloys with improved specific strength and damage tolerance and reduced mechanical property anisotropy [1]. This interest stemmed from the fact that each 1.0% lithium added to the alloy reduced its density by 3.0% and increased the elastic modulus by approximately 5.0% [2]. A representative 3rd generation Al–Li alloy is the AF/C 458 alloy, which was developed in 1997 and designated as AA 2099 by the Aluminum Association in 2004 [3]. Research data indicate that 2099 alloy has superior physical and mechanical properties over traditional 2000 and 7000 series aluminum alloys, and it overcomes many shortcomings, especially mechanical anisotropy, of previous Al–Li alloys [4]. The 2099 alloy was selected because it was a candidate for several production applications. Among current Al–Li alloys, 2099 Al–Li alloy has the highest modulus and lowest density with

good strengths [5]. A thorough study on hot deformation behavior of this material is essential to properly design the thermo-mechanical process parameter as it directly affects the microstructure evolution and consequently, the mechanical properties of the formed product [6].

The application of 2099 alloy, despite of its remarkable mass saving potential, is still somewhat limited due to its inferior mechanical properties, such as strength and ductility. In this regard, the successful use of thermo-mechanical processing methods to improve the mechanical properties of 2099 alloy is largely responsible for the recent increased interest in the development of proper constitutive models. Heretofore, the previous studies on analyzing the constitutive behavior of aluminum alloys have been principally limited to the effects of temperature and strain rate. But recently a revised hyperbolic sine constitutive equation has been proposed to predict the high-temperature flow behavior by taking the effect of strain into account. This method has been employed in order to formulate the constitutive behaviors of pure aluminum [7], Cr₂₀Ni₂₅Mo₄Cu superaustenitic stainless steel [8], Ti-modified austenitic stainless steel [9], 7075

aluminum alloy [10] and Al–14Cu–7Ce alloy [11]. In the past few years, many researchers have paid attention to this alloy, especially in terms of its microalloying, aging process and failure behavior [1–5,12,13]. However, there is a lack of knowledge on the strain dependent constitutive analysis of 2099 alloy.

The objective of this study is to formulate a suitable constitutive relationship to evaluate and predict the effect of process parameters on high-temperature flow behavior of 2099 alloy considering the strain effects. To achieve this purpose, isothermal hot compression tests were conducted in a wide range of strain rates and temperatures. The experimental data were corrected and then employed to determine the material constants in the constitutive relation and thereby correlating flow stress, strain, strain rate and temperature. Finally, the predictability of the established constitutive modeling was verified over the entire experimental range.

2 Experimental

An as-cast 2099 alloy ingot ($d540\text{ mm}\times 1000\text{ mm}$) homogenized at (515 °C, 18 h)+(525 °C, 16 h), with the composition given in Table 1, was used as experimental material. The optical micrograph of the homogenized material is shown in Fig. 1. The microstructure consists of coarse equiaxed $\alpha(\text{Al})$ grains along with a small amount of the second phase particles at some grain boundaries. Cylindrical specimens with 10 mm in diameter and 15 mm in height were machined from the homogenized ingot to carry out the compression testing. In order to reduce the friction between the specimens and the dies during hot deformation, the flat ends of each specimen were recessed a pair of circular grooves with diameter of 9 mm and depth of 0.2 mm to entrap the

Table 1 Chemical composition of experimental 2099 alloy (mass fraction, %)

Cu	Li	Zn	Mg	Mn	Zr	Al
2.6	1.75	0.64	0.29	0.3	0.08	Bal.

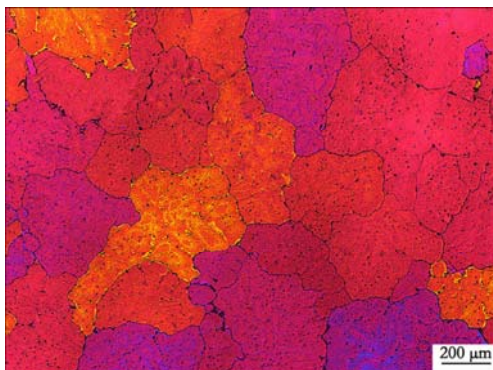


Fig. 1 Optical microstructure of 2099 alloy after homogenizing at (515 °C, 18 h)+(525 °C, 16 h)

lubricant of hexagonal BN with graphite foil. Hot compression tests were conducted on a Gleeble–1500 thermo-mechanical simulator in the temperatures range from 300 to 500 °C at an interval of 40 °C and at constant true strain rates of 0.001, 0.01, 0.1, 1 and 10 s^{-1} . Prior to the tests, the specimens were soaked at deformation temperature for 3 min and the deformations were continued up to the true strain of 0.7. Finally, at the end of straining the specimens were immediately quenched in water.

3 Results and discussion

3.1 Friction correction

In this study, although lubricants were used to minimize the interfacial friction, the interfacial friction becomes more and more evident with the increase of deformation. Thus, the deformation is more and more heterogeneous, leading to the drum-like shape of specimens. Therefore, the measured flow stress should be corrected with the friction.

Some works have been done about friction correction for hot deformation [14,15], and most of them need to measure the height and the maximum radius of specimens after deformation. Due to measurement error the friction corrected flow stress cannot accurately characterize the flow behavior.

The longitudinal changes of the specimen in the process of hot compression can be described by the displacement–load curve, which assumes that the specimen deformation is uniform (i.e. no drum-like appears). Therefore, the true stress–true strain curve can be calculated by equivalent calculation employing the displacement–load data, which can characterize the flow behavior more reasonably.

According to definition of the true stress–true strain, there are expressions:

$$\sigma = F_i/A_i \tag{1}$$

$$\varepsilon = \ln[(h_0 - \Delta h)/h] \tag{2}$$

where F_i and A_i are the instantaneous load and the cross-sectional area, respectively; h_0 is the original height; $\Delta h = h_0 - h_i$ (h_i is the instantaneous height). Plastic deformation of the metallic materials is a constant volume process, that is the identity $A_0 h_0 = A_i h_i$, A_0 is the original cross-sectional area of a specimen. Hence, A_i can be described as

$$A_i = \frac{\pi D_0^2 h_0}{4(h_0 - \Delta h)} \tag{3}$$

Taking Eq. (3) into Eq. (1) would yield the following equation:

$$\sigma = \frac{4F_i(h_0 - \Delta h)}{\pi h_0 D_0^2} \tag{4}$$

where D_0 is the original diameter of the specimen. Based on the specimen size used in the test, the true stress and true strain can be simplified as

$$\begin{cases} \sigma = 0.83F_i(1.5 - \Delta h) \\ \varepsilon = \ln[1.5/(1.5 - \Delta h)] \end{cases} \quad (5)$$

The original and the friction corrected flow stresses at the strain rates of 0.1 s^{-1} and 1 s^{-1} are shown in Figs. 2(a) and (b), respectively. It can be observed that the original stresses are greater than the friction corrected ones, and become more and more obviously with the decrease of temperature and the increase of strain. This phenomenon demonstrates that the friction has an important influence on the deformation, especially in the condition of low temperature and large deformation.

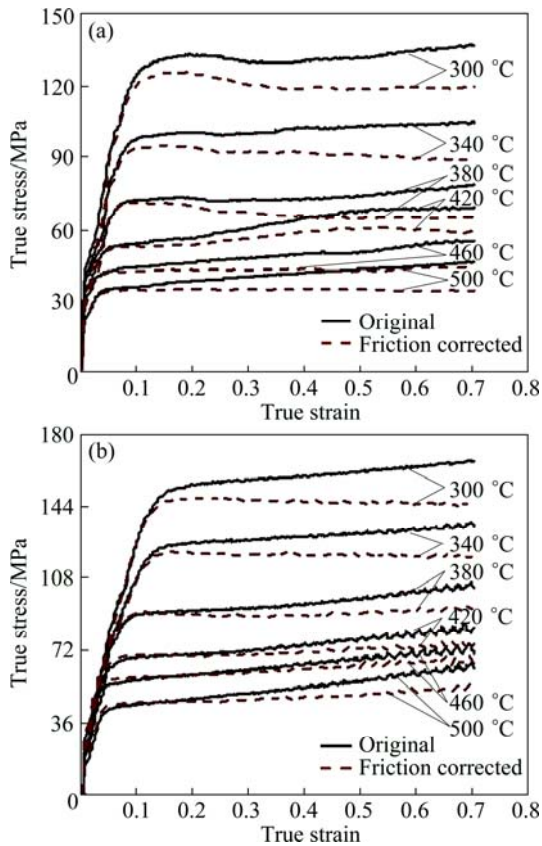


Fig. 2 Original and friction corrected stress curves at strain rates of 0.1 s^{-1} (a) and 1 s^{-1} (b)

3.2 Temperature correction

Softening behavior in the process of thermal deformation is mainly caused by deformation heat and structural changes. In this study, although a compression test conducted under the isothermal condition used a heating unit of the Gleeble 1500, the specimen temperature rise was still up to about $10 \text{ }^\circ\text{C}$ in the high speed deformation conditions. Therefore, the measurement temperature was used rather than the nominal heating temperature for data processing in this study.

The relationship between the flow stress and strain rate at high stress levels and low stress levels for the thermal deformation of different materials can be presented respectively as [16,17]

$$Z = A_1 \sigma^{n_1} = \dot{\varepsilon} \exp(Q/(RT)) \quad (\text{low-stress level}) \quad (6)$$

$$Z = A_2 \exp(\beta\sigma) = \dot{\varepsilon} \exp(Q/(RT)) \quad (\text{high-stress level}) \quad (7)$$

where Z is the Zener–Hollomon parameter, σ is the flow stress; R is the gas constant; T is the thermodynamic temperature; Q is the activation energy; A_1, A_2, n_1 and β are the material constants, which are experimentally determined.

Assuming that the Q value is a constant within a certain temperature range. In a particular strain rate condition, taking the logarithm of both sides of Eqs. (6) and (7) leads to the following formulas:

$$\ln \sigma = B_1 + 1000/(C_1 T) \quad (8)$$

$$\sigma = B_2 + 1000/(C_2 T) \quad (9)$$

where

$$B_1 = \frac{\ln \dot{\varepsilon} - \ln A_1}{n_1},$$

$$B_2 = \frac{\ln \dot{\varepsilon} - \ln A_2}{\beta},$$

$$C_1 = \frac{1000 n_1 R}{Q},$$

$$C_2 = \frac{1000 \beta R}{Q}$$

which can be calculated by the measurement temperature and corrected flow stress to conduct a linear fitting. Then, taking the nominal temperature into Eqs. (8) and (9), the temperature corrected flow stress can be obtained. The temperature correction method does not consider the strain, so the flow stress should be corrected under different strain conditions.

To investigate the effect of temperature changes on the flow stress of 2099 alloy, the flow stress curves at the strain rates of 0.1 s^{-1} and 1 s^{-1} are shown in Figs. 3(a) and (b), respectively. As is seen, the flow stress is significantly affected by temperature and strain rate. At high temperatures and low strain rates, the deformation process is close to isothermal conditions. Hence, the curves of friction corrected and friction–temperature corrected are agreement with each other basically. However, the difference becomes very significant at low temperatures and high strain rates due to temperature rising effect at 1 s^{-1} and $300 \text{ }^\circ\text{C}$.

3.3 Determination of material constants

Based on the corrected experimental true stress–true strain data, constitutive equations are commonly used to determine the material constants during hot deformation process.

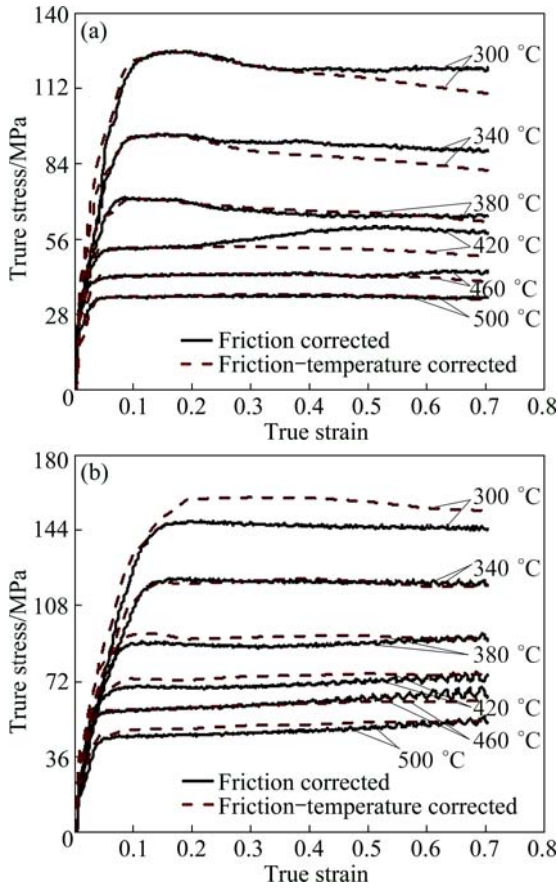


Fig. 3 Flow stress curves between friction corrected and friction-temperature corrected ones: (a) 0.1 s⁻¹; (b) 1 s⁻¹

The hyperbolic sine-type equation, proposed by SELLARS and MCTEGART [18], has been extensively employed to characterize the relationship between deformation parameters in a broad range of stress:

$$Z = A[\sinh(\alpha\sigma)]^n = \dot{\epsilon} \exp[Q/(RT)], \quad \text{for all stress level} \quad (10)$$

where A is structure factor; α is stress level parameter; n is stress exponent. Taking the logarithm of both sides of Eq. (10) leads to

$$\ln \dot{\epsilon} = n \ln[\sinh(\alpha\sigma)] + \ln A - Q/(RT) \quad (11)$$

The value of α is derived by β/n_1 . These two material constants, β and n_1 , are deduced through taking the logarithm of both sides of Eqs. (6) and (7), at a constant temperature:

$$\ln \dot{\epsilon} = n_1 \ln \sigma + \ln A_1 - Q/(RT) \quad (12)$$

$$\ln \dot{\epsilon} = \beta \sigma + \ln A_2 - Q/(RT) \quad (13)$$

Then, the flow stress and its corresponding strain rate are substituted into Eqs. (12) and (13) under the true strain of 0.1, respectively. By linear regression for the data points, the relationships between flow stress and strain rate are obtained, as shown in Fig. 4. The values of

n_1 and β can be obtained by averaging slope values of the lines from 420 to 500 °C in Fig. 4(a) and from 300 to 380 °C in Fig. 4(b), respectively. Therefore, the α value is calculated to be 0.01513 MPa⁻¹.

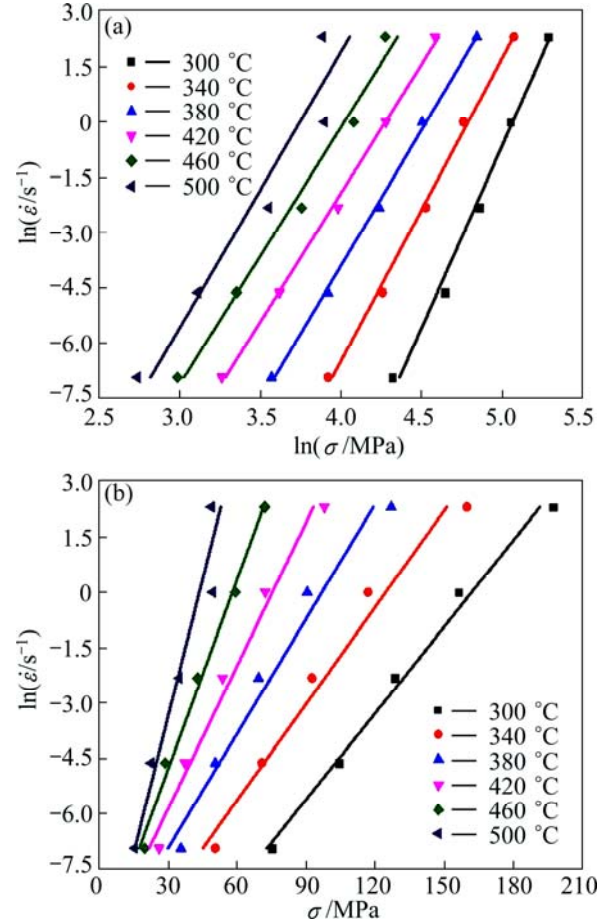


Fig. 4 Relationships between strain rate and flow stress: (a) $\ln \sigma - \ln \dot{\epsilon}$; (b) $\sigma - \ln \dot{\epsilon}$

For a particular strain rate, differentiating Eq. (11) gives

$$Q = Rns \quad (14)$$

where

$$n = \left\{ \frac{\partial \ln \dot{\epsilon}}{\partial \ln[\sinh(\alpha\sigma)]} \right\}_T \quad (15)$$

$$s = \left\{ \frac{\partial \ln[\sinh(\alpha\sigma)]}{\partial (1/T)} \right\}_{\dot{\epsilon}} \quad (16)$$

Therefore, by substituting the flow stress, temperature and corresponding strain rate into Eqs. (15) and (16), the slope values in the plots of $\ln \dot{\epsilon} - \ln[\sinh(\alpha\sigma)]$ and $\ln[\sinh(\alpha\sigma)] - 1000/T$ can be obtained, as shown in Figs. 5(a) and (b). Then, the Q value can be derived from the calculated mean slope of lines in the $\ln \dot{\epsilon} - \ln[\sinh(\alpha\sigma)]$ and $\ln[\sinh(\alpha\sigma)] - 1000/T$ plots respectively, and evaluated as 203.249 kJ/mol at the true strain of 0.1.

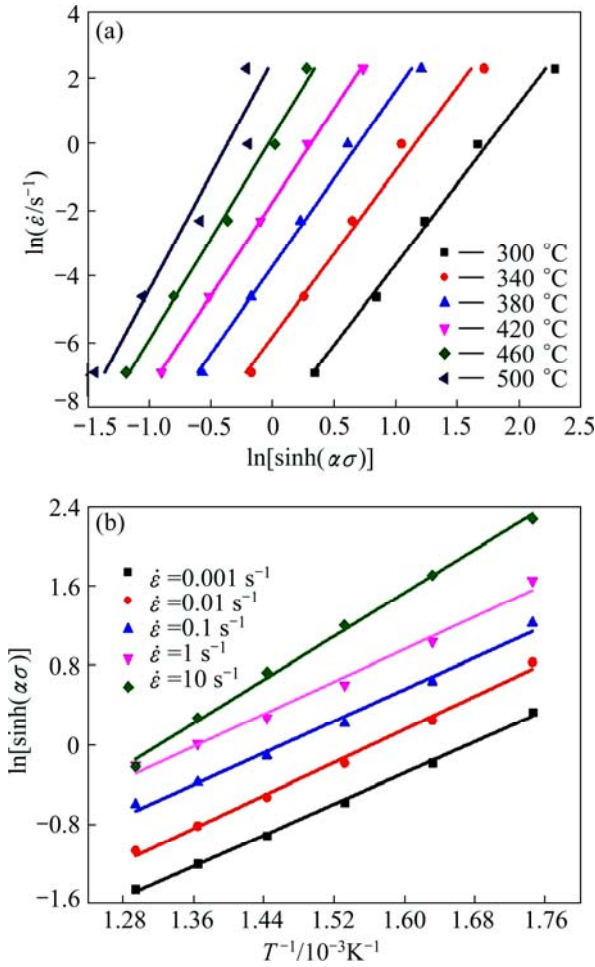


Fig. 5 Relationships between flow stress with strain rate and temperature: (a) $\ln \dot{\epsilon} - \ln[\sinh(\alpha\sigma)]$; (b) $\ln[\sinh(\alpha\sigma)] - 1000/T$

Furthermore, substituting the values of Q , $\dot{\epsilon}$ and T into Eq. (10), the values of Z at different deformation temperatures and strain rates can be obtained. The value of A (approximately $3.54 \times 10^{14} \text{ s}^{-1}$) at the true strain of 0.1 could be computed by the relationship of $\ln Z - \ln[\sinh(\alpha\sigma)]$ (Fig. 6), and more accurate n value (about 5.5468) can be obtained.

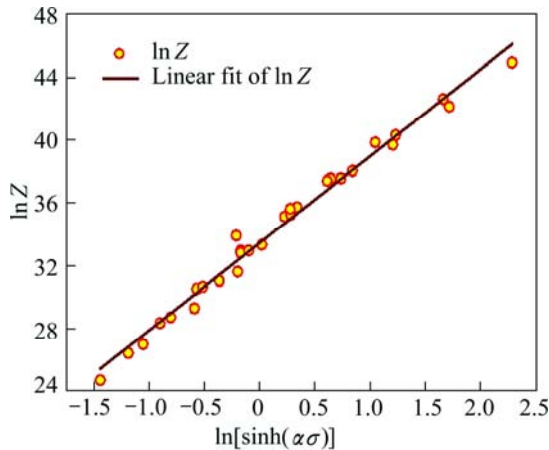


Fig. 6 Relationship between flow stress and Z parameter

3.4 Compensation of strain

It is assumed that influence of strain on high-temperature deformation behavior is insignificant and thereby it is not considered in Eq. (10). However, as demonstrated in Figs. 2 and 3, the effect of strain is significant in the lower thermal deformation temperature regime. Hence, compensation of strain should be taken into account in order to develop the proper constitutive equations which accurately predict the flow behavior.

In order to incorporate the influence of strain in the constitutive equation, it is assumed that the material constants are polynomial functions of strain [19]. The values of material constants of the constitutive equations were calculated at various strains ranging from 0.1 to 0.7 at an interval of 0.1 in this work, as listed in Table 2. Then, these values are employed to fit the polynomial. Finally, an eighth-order polynomial, as shown in Fig. 7, is found to represent the influence of the strain on material constants with a very good correlation and generalization for 2099 alloy. The polynomial fit results of α , Q , n and $\ln A$ of 2099 alloy are listed in Table 2.

Table 2 Values of material constants of 2099 alloy

ϵ	α/MPa^{-1}	$Q/(\text{kJ}\cdot\text{mol}^{-1})$	n	$\ln(A/\text{s}^{-1})$
0.1	0.015131	203.249	5.5468	33.50203
0.2	0.015244	202.0968	5.46382	33.3193
0.3	0.015894	188.0716	5.20625	30.61355
0.4	0.015447	186.9371	5.27539	30.54529
0.5	0.015781	176.0727	5.03225	28.54546
0.6	0.015937	169.9869	4.94949	27.46611
0.7	0.016033	167.3693	4.96089	26.99184

Once the material constants are evaluated, the flow stress at a particular strain can be predicted. According to the definition of the hyperbolic law, the flow stress can be written as a function of the Z parameter. Combined with Eq. (10), the constitutive equations for hot deformation behavior of 2099 alloy can be summarized as follows:

$$\begin{cases} \sigma = \frac{1}{\alpha} \ln \left\{ (Z/A)^{1/n} + [(Z/A)^{2/n} + 1]^{1/2} \right\} \\ Z = \dot{\epsilon} \exp[Q/(RT)] \\ \alpha = \alpha_0 + \alpha_1 \epsilon + \alpha_2 \epsilon^2 + \alpha_3 \epsilon^3 + \dots + \alpha_8 \epsilon^8 \\ n = n_0 + n_1 \epsilon + n_2 \epsilon^2 + n_3 \epsilon^3 + \dots + n_8 \epsilon^8 \\ Q = Q_0 + Q_1 \epsilon + Q_2 \epsilon^2 + Q_3 \epsilon^3 + \dots + Q_8 \epsilon^8 \\ \ln A = A_0 + A_1 \epsilon + A_2 \epsilon^2 + A_3 \epsilon^3 + \dots + A_8 \epsilon^8 \end{cases} \quad (17)$$

3.5 Verification of developed constitution equations

In order to evaluate the accuracy of the developed constitutive equations (considering the compensation of strain) in predicting the thermal deformation behavior of

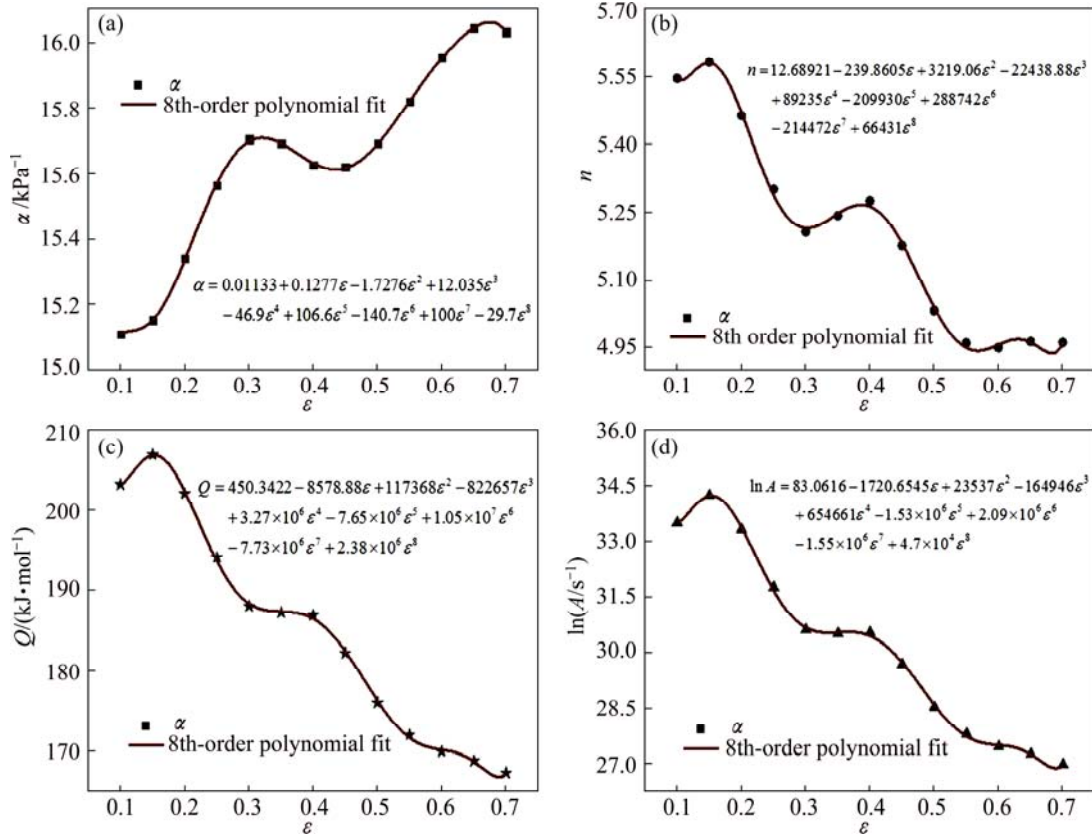


Fig. 7 Variations of α (a), n (b), Q (c) and $\ln A$ (d) with true strain based on 8th-order polynomial fit for 2099 alloy

2099 alloy, a comparison between the corrected and the predicted flow stress from the constitutive equations at various processing conditions is shown in Fig. 8. As is observed, the predicted flow stress from the developed constitutive equations could track the corrected flow stress throughout the entire experimental conditions in this work.

Moreover, the predictability of the developed constitutive equations is further verified employing standard statistical parameters such as correlation coefficient (R^2) and average relative error (E_r). These formulae are as follows:

$$R^2 = \frac{\sum_{i=1}^N (\sigma_c^i - \bar{\sigma}_c)(\sigma_p^i - \bar{\sigma}_p)}{\sqrt{\sum_{i=1}^N (\sigma_c^i - \bar{\sigma}_c)^2} \sqrt{\sum_{i=1}^N (\sigma_p^i - \bar{\sigma}_p)^2}} \quad (18)$$

$$E_r = \frac{1}{N} \sum_{i=1}^N \left| \frac{\sigma_c^i - \sigma_p^i}{\sigma_c^i} \right| \quad (19)$$

where σ_c^i is the corrected flow stress; σ_p^i is the predicted flow stress; $\bar{\sigma}_c$ and $\bar{\sigma}_p$ are the mean values of σ_c^i and σ_p^i , respectively; N is the total number of data. The correlation coefficient is representative of the strength of linear relationship between the corrected and predicted values. Sometimes higher values of R^2 may not

necessarily indicate a better performance because of the tendency of the model to be biased towards higher or lower values. The E_r is computed through a term-by-term comparison of the relative error and therefore is an unbiased statistical parameter for measuring the predictability of a model [9]. In the present work, as shown in Fig. 9, the values of R^2 and E_r are calculated to be 99.8% and 2.04%, respectively. This implies the excellent predictability of the proposed constitutive model.

4 Conclusions

1) In order to characterize the flow behavior accurately during hot deformation, the flow stress was modified by the friction and temperature correction. The corrected flow stress is strongly dependent on deformation temperature and strain rate, which increases with decreasing temperature and increasing strain rate.

2) The results show that strain has a significant influence on the flow stress. Hence, the influence of strain in the constitutive analysis is incorporated by considering the effect of strain on material constants (α , n , Q and A). The 8th-order polynomial fitting equations were found to represent the influence of strain on these material constants with very good correlation and generalization.

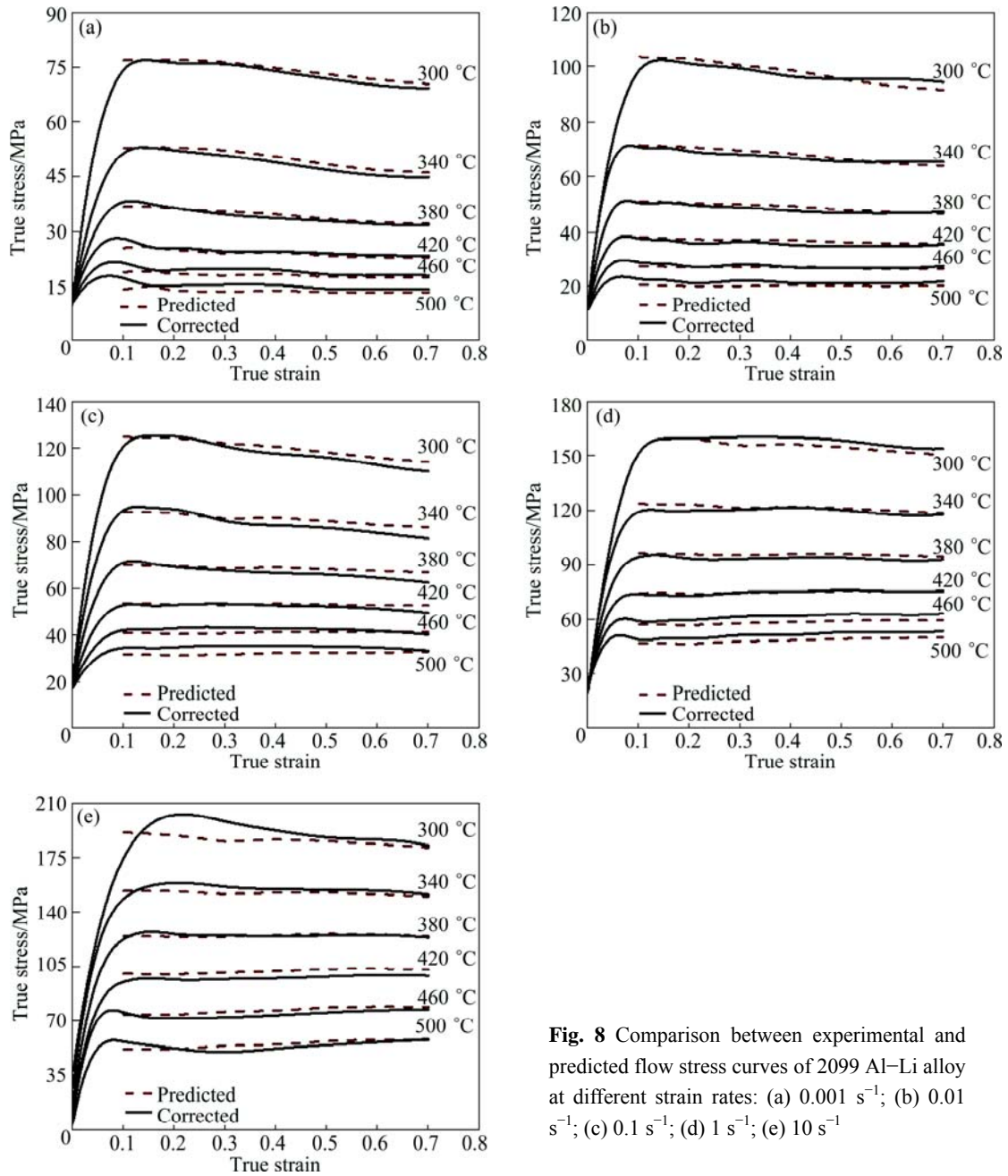


Fig. 8 Comparison between experimental and predicted flow stress curves of 2099 Al-Li alloy at different strain rates: (a) 0.001 s^{-1} ; (b) 0.01 s^{-1} ; (c) 0.1 s^{-1} ; (d) 1 s^{-1} ; (e) 10 s^{-1}

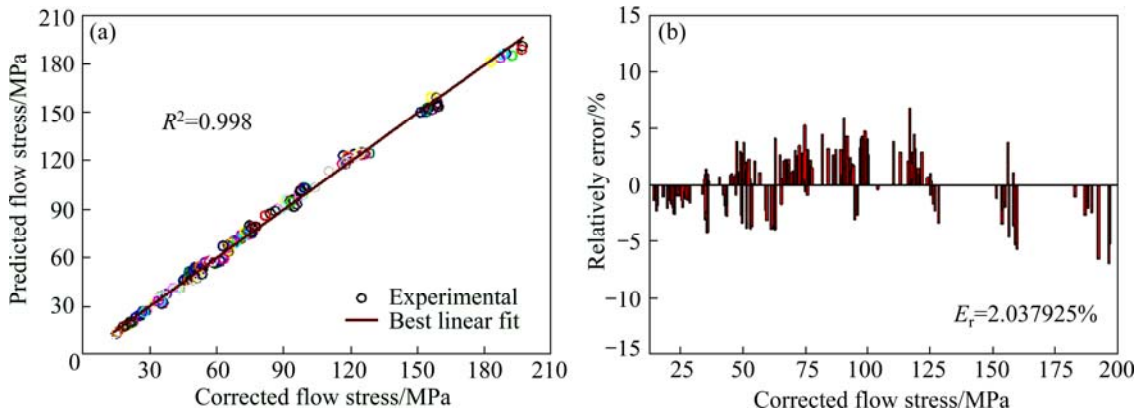


Fig. 9 Statistic analysis of results: (a) Correlation between experimental and predicted flow stress; (b) Relative error by constitutive equations

3) The reliability of developed constitutive equation, incorporating the strain compensation, was assessed using standard statistical method. The results demonstrate that the developed constitutive equations give a precise estimate for the flow stress and can be used to numerically simulate the hot deformation of 2099 alloy.

References

- [1] FRAGOMENI J, WHEELER R, JATA K V. Effect of single and duplex aging on precipitation response, microstructure, and fatigue crack behavior in Al–Li–Cu alloy AF/C-458 [J]. JMEPEG, 2005, 14(1): 18–27.
- [2] JABRA J, ROMIOS M, LAI J, LEE E, SETIAWAN M, LEE E W, WITTERS J, ABOURIALY N, OGREN J R, CLARK R, OPPENHEIM T, FRAZIER W E, ES-SAID O S. The effect of thermal exposure on the mechanical properties of 2099-T6 die forgings, 2099-T83 extrusions, 7075-T7651 plate, 7085-T7452 die forgings, 7085-T7651 plate, and 2397-T87 plate aluminum alloys [J]. JMEPEG, 2006, 15(5): 601–607.
- [3] MA Y, ZHOU X, THOMPSON G E, HASHIMOTO T, THOMSON P, FOWLES M. Distribution of intermetallics in an AA 2099-T8 aluminium alloy extrusion [J]. Materials Chemistry and Physics, 2011, 126(1–2): 46–53.
- [4] ROMIOS M, TIRASCHI R, PARRISH C, BABEL H W, OGREN J R, ES-SAID O S. Design of multistep aging treatments of 2099 (C458) Al–Li alloy [J]. JMEPEG, 2005, 14(5): 641–646.
- [5] BABEL H, GBSON J, TARKANIAN M, PARRISH C, PRIETTO M, ORDONEZ-CHU A, HABERL H, KABISCH J, CLARK R, OGREN J, ES-SAID O S. 2099 aluminum–lithium with key-locked inserts for aerospace applications [J]. JMEPEG, 2007, 16(5): 584–591.
- [6] LI H Y, WEI D D, HU J D, LI Y H, CHEN S L. Constitutive modeling for hot deformation behavior of T24 ferritic steel [J]. Computational Materials Science, 2012, 53(1): 425–430.
- [7] REZAEI ASHTIANI H R, PARSANI M H, BISADI H. Constitutive equations for elevated temperature flow behavior of commercial purity aluminum [J]. Materials Science and Engineering A, 2012, 545: 61–67.
- [8] HAN Y, QIAO G J, SUN Y, ZOU D N. Modeling the constitutive relationship of Cr₂₀Ni₂₅Mo₄Cu superaustenitic stainless steel during elevated temperature [J]. Materials Science and Engineering A, 2012, 539: 61–67.
- [9] MANDAL S, RAKESH V, SIVAPRASAD P V, VENUGOPAL S, KASIVISWANATHAN K V. Constitutive equations to predict high temperature flow stress in a Ti-modified austenitic stainless steel [J]. Materials Science and Engineering A, 2009, 500(1–2): 114–121.
- [10] ROKNI M R, ZAREI-HANZAKI A, ROOSTAEI A A, AOLHASANI A. Constitutive base analysis of a 7075 aluminum alloy during hot compression testing [J]. Materials and Design, 2011(10), 32: 4955–4960.
- [11] LI W, LI H, WANG Z X, ZHENG Z Q. Constitutive equations for high temperature flow stress prediction of Al–14Cu–7Ce alloy [J]. Materials Science and Engineering A, 2011(12), 528: 4098–4103.
- [12] WEI Xiu-yu, ZHENG Zi-qiao, SHE Ling-juan, CHEN Qiu-ni, LI Shi-chen. Microalloying roles of Mg and Zn additions in 2099 Al–Li alloy [J]. Rare Metal Materials and Engineering, 2010, 39(9): 1583–1587. (in Chinese)
- [13] WARD N, TRAN A, ABAD A, LEE E W, HAHN M, FORDAN E, ES-SAID O S. The effects of retrogression and reaging on aluminum alloy 2099 (C458) [J]. JMEPEG, 2011, 20(6): 989–996.
- [14] EBRAHIMI R, NAJAFIZADEH A. A new method for evaluation of friction in bulk metal forming [J]. Journal of Materials and Processing Technology, 2004, 152(2): 136–143.
- [15] LIANG X P, LIU Y, LI H Z, ZHOU C X, XU G F. Constitutive relationship for high temperature deformation of powder metallurgy Ti–47Al–2Cr–2Nb–0.2W alloy [J]. Materials and Design, 2012, 37: 40–47.
- [16] McQUEEN H J, RYAN N D. Constitutive analysis in hot working [J]. Materials Science and Engineering A, 2002, 322(1–2): 43–63.
- [17] MIRZADEHA H, CABRERA J M, PRADO J M, NAJAFIZADEH A. Hot deformation behavior of a medium carbon microalloyed steel [J]. Materials Science and Engineering A, 2011, 528(10–11): 3876–3882.
- [18] SELLARS C M, McTEGART W J. On the mechanism of hot deformation [J]. Acta Metallurgica, 1996, 14(9): 1136–1138.
- [19] LIN Y C, CHEN M S, ZHONG J. Effect of temperature and strain rate on the compressive deformation behavior of 42CrMo steel [J]. Journal of Materials and Processing Technology, 2008, 205(1–3): 308–315.

考虑应变因素的 2099 合金高温流变行为模型

张 飞^{1,2}, 沈 健¹, 闫晓东¹, 孙建林², 孙晓龙¹, 杨 银¹, 刘 勇³

1. 北京有色金属研究总院, 北京 100088; 2. 北京科技大学 材料科学与工程学院, 北京 100083;
3. 南方航空动力机械集团有限公司, 株洲 412000

摘 要: 采用等温热压缩试验研究 2099 合金在变形温度 300~500 °C、应变速率 0.001~10 s⁻¹ 条件下的热变形行为。为了准确地表征流变行为, 采用摩擦与温度修正后的实验数据构建本构模型。结果表明, 温度和应变速率对合金热变形行为的影响可用包含 Arrhenius 关系的 Z 参数来表征。此外, 通过计算不同应变率下的材料常数(α 、 n 、 Q 和 A)考虑了应变对本构模型的影响。利用统计分析对比了由本构模型获得的预测曲线与试验修正曲线, 二者显示了很好的吻合, 这表明所构建的本构模型能够很好地预测 2099 合金的热变形流变行为。

关键词: 2099 合金; 本构模型; 补偿应变; 流变应力